Nisha Shukla, Puneet Rana*, and O. Anwar Bég

Unsteady MHD Non-Newtonian Heat Transfer Nanofluids with Entropy Generation Analysis

https://doi.org/10.1515/nleng-2017-0177
Received November 7, 2017; revised May 1, 2018; accepted June 7, 2018.

Abstract: A theoretical study of unsteady magnetohydrodynamic boundary layer stagnation point flow, heat and mass transfer of a second grade electrically-conducting nanofluid from a horizontal stretching sheet with thermal slip and second order slip velocity effects is presented. The Buongiorno formulation is employed for nanofluids and in addition the no-flux nanoparticle boundary condition is also considered. The appropriate similarity transformations are applied to convert the governing equations into the system of nonlinear partial differential equations, which is solved by using homotopy analysis method. Entropy generation and Bejan number have also been evaluated for the effects of magnetic parameter, Reynolds number and slip parameter in non-Newtonian (second-grade) time-dependent flow. The computations show that skin friction coefficient and entropy generation number increase with an increment in magnetic parameter whereas Bejan number decreases with it. Local Nusselt number decreases with an increase in the value of Eckert number (viscous dissipation) and thermal slip whereas the converse behaviour is captured for velocity parameter. The work is relevant to magnetohydrodynamic nanomaterials processing.

Keywords: Unsteady flow; Heat and mass transfer; Magnetohydrodynamics; Non-Newtonian nanofluid; Stretching sheet; HAM solutions; Entropy; Bejan number

Nisha Shukla, Department of Mathematics, Jaypee Institute of Information Technology, A-10, Sector-62, Noida-201307, Uttar Pradesh, India

***Corresponding Author: Puneet Rana,** Department of Mathematics, Jaypee Institute of Information Technology, A-10, Sector-62, Noida-201307, Uttar Pradesh, India, E-mail: puneetranaiitr@gmail.com

O. Anwar Bég, Fluid Mechanics, Propulsion and Nanosystems, Aeronautical and Mechanical Engineering, School of Computing, Science & Engineering, University of Salford, Newton Building, M54WT, UK

1 Introduction

Non-Newtonian fluid flows feature in an extensive range of technological applications including polymer processing, wire coating, food manufacture, biological fluids movement, hot rolling, fibre technology, crystal growth and petroleum purification [1, 2]. Nanofluids [3–9] are fluids which contains suspended nanoparticles (for example Al_2O_3, CuO, SiC) in a base fluid (water, lubricants and organic liquids). Rana *et al.* [10] have examined the MHD slip flow of Al_2O_3–water nanofluid over a horizontal shrinking cylinder. Non-Newtonian fluids are characterized into some subclasses according to their diverse properties. Each class may be characterized by a constitutive equation. One such category is viscoelastic fluids which display both elastic and viscous properties over a wide range of shear rates. They may also exhibit normal stress differences, relaxation, retardation, memory effects and so on. A subclass of non-Newtonian viscoelastic fluids is the differential second grade Rivlin-Ericksen fluid which quite accurately simulates normal stress effects. This non-Newtonian model has therefore stimulated substantial interest in rheological fluid mechanics. The non-Newtonian properties of certain nanofluids also allow the second grade model to be utilized in describing their shear stress-strain characteristics. Erdogan and Imrak [11] presented an exact solution for steady incompressible second grade nanofluid flow which passage through a rotating porous cylinder. Zhang *et al.* [12] have applied an inverse method to obtain exact solutions for steady second grade fluid flow. Rana and Bhargava [13] have applied a variational finite element method to compute velocity and temperature field solutions for steady viscoelastic second grade nanofluid flow and heat transfer from a stretching surface. They observed that wall heat transfer rate increases with an increment in viscoelastic parameter. Khurana *et al.* [14] have investigated the influence of magnetic field on non-Newtonian nanofluid layer. Both linear and nonlinear analysis has been explored by considering stress free boundary conditions on the flow confined between parallel plates.

Magnetohydrodynamics (MHD) has emerged as a growing area in modern engineering sciences and involves

the interaction between flowing electrically-conducting fluids and static or dynamic magnetic fields. It arises in the design of MHD accelerators and power generators [15, 16] electromagnetic blood flow meters, metallurgical (liquid metal) processing, nuclear cooling systems, magnetic materials synthesis and etc. Many complex phenomena are generated in MHD boundary layer flows including Lorentzian body force, Ohmic dissipation, Hall currents and magnetic induction. *Magnetic nanofluids* combine the responsiveness of electrically-conducting fluids to electromagnetic fields and the thermal enhancement properties of nanofluids. Many researchers have studied the boundary layer transport phenomena in such fluids. Recently, Dhanai *et al.* [17] derived dual solutions for MHD boundary layer flow of a power-law non-Newtonian nanofluid from a porous nonlinear shrinking sheet with heat source or sink effects. Rana *et al.* [18] have also captured the multiple solutions in the study of non-Newtonian nanofluid flow induced by shrinking sheet. Temporal stability analysis has been implemented to confirm the stability of the solutions.

A point in a fluid at which the local velocity of fluid becomes zero is termed a *stagnation point*. Historically Hiemenz [19] first investigated stagnation point flow for Newtonian viscous fluids. The presence of stagnation-point flows in coating flows and other materials manufacturing operations has stimulated considerable interest in this type of flow in recent years. Hayat *et al.* [20] investigated heat and mass transfer in MHD stagnation point flow of a second grade nanofluid over a permeable stretching cylinder. Reddy and Sankar [21] investigate numerically the effects of heat source suction and viscous dissipation on MHD stagnation point flow of a steady, viscous and incompressible nanofluid past an exponentially stretching sheet. Bachok *et al.* [22] and also Suali *et al.* [23] considered the unsteady stagnation point flow and heat transfer of a nanofluid over a stretching sheet. Abbas *et al.* [24] computed multiple solutions for steady MHD boundary layer stagnation point nanofluid flow from a stretching sheet with homogeneous-heterogeneous chemical reactions. Rana *et al.* [25] have used the Lie group analysis to find similarity transformations for the study of stagnation point flow of nanofluid over a nonlinear shrinking surface.

The preceding studies have generally omitted consideration of second order velocity (hydrodynamic) wall slip and thermal slip effects. Partial slip conditions provide better results as compared to no-slip conditions, as elaborated by Yoshimura and Prudhomme [26] and Zhu and Granick [27] who have included non-zero *first order* derivatives of velocity at the boundary. However for the case of large Knudsen number, it is necessary to incorporate *second order* derivatives in order to improve the accuracy of computations and correlation with actual physical phenomena [28]. The second order slip condition has been shown to exert a significant effect in non-Newtonian nanofluid flows. Some authors [29, 30] have calculated dual or multiple solutions in such type of flow models.

In any thermodynamic process *entropy* can be generated due to heat transfer across finite temperature gradients, Joule heating (Ohmic dissipation), mass diffusion and viscous dissipation. Engineers may successfully optimize a thermal engineering system with higher energy efficiency by minimizing entropy generation in system [31]. Entropy generation analysis has a wide range of applications in different fields such as heat exchangers, porous media, combustion, high temperature gas turbine dynamics, gas turbine regenerators etc. [32–34]. Bejan [35] has introduced a general methodology for entropy generation analysis for forced convective heat transfer over a plate and circular cylinder. This entropy generation minimization approach has been applied by many authors [36–41] in a wide spectrum of thermofluid systems.

The main motivation of this article is to solve analytically the system of nonlinear partial differential equations arising in unsteady MHD boundary layer stagnation point flow of second grade nanofluid from a horizontal stretching sheet with second order slip velocity and thermal slip effects. An entropy generation analysis is also included. The transformed, two-dimensional nonlinear boundary value problem is solved with the powerful homotopy analysis method (HAM) [42, 43] which is a power-series based hybrid analytical/numerical technique for solving very efficiently systems of ordinary or nonlinear partial differential equations. Many researchers have employed HAM in simulating a range of complex, multi-physical transport problems [44–47]. Extensive graphical solutions are presented. Validation of HAM solutions with earlier studies is also included. The present work is relevant to providing a deeper insight into hydromagnetic thermal, momentum and species transfer characteristics in stagnation point flows of non-Newtonian electro-conductive nanopolymers and has not been investigated in the literature, thus far, to the authors' knowledge.

2 Problem Formulation

The unsteady laminar two-dimensional MHD stagnation point boundary layer flow of an incompressible, electro-conductive, viscoelastic second grade nanofluid over a stretching sheet is considered. The stagnation point O is assumed to be fixed at $x = y = 0$. It is assumed that the

stretching velocity of the sheet is $u_w = bx$ whereas the ambient velocity of fluid is $u_\infty = ax$. The *x-axis* is orientated along the sheet and the *y-axis* is perpendicular to the sheet. The direction of applied magnetic field B_0 is assumed to be normal to the heated surface having temperature T_w ($T_w > T_\infty$).

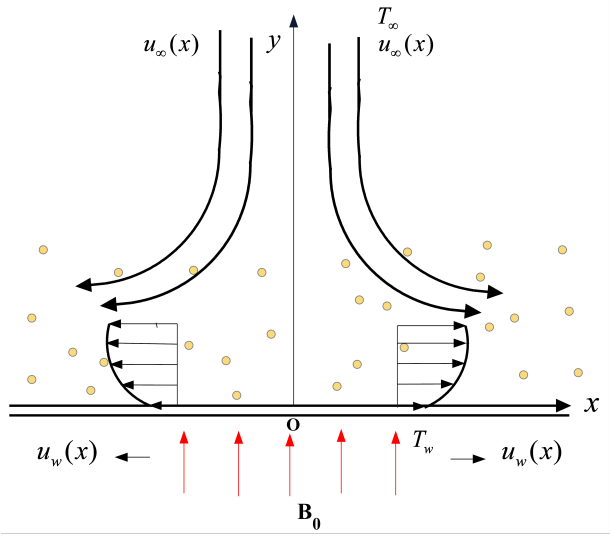

Fig. 1: Physical model and co-ordinate system for MHD nanofluid stagnation point flow.

The flow regime is visualized with the associated co-ordinate system in Fig. 1. The governing equations are defined [20, 48] as follows:

Continuity Equation:

$$\frac{\partial u}{\partial x} + \frac{\partial u}{\partial y} = 0, \tag{1}$$

Momentum equation:

$$\frac{\partial u}{\partial t} + u\frac{\partial u}{\partial x} + v\frac{\partial u}{\partial y} = \frac{\partial u_\infty}{\partial t} + u_\infty \frac{du_\infty}{dx} + \upsilon_{nf}\frac{\partial^2 u}{\partial y^2} + \frac{\alpha_1}{\rho_{nf}}\left[\frac{\partial^3 u}{\partial t \partial y^2} + \frac{\partial}{\partial x}\left(u\frac{\partial^2 u}{\partial y^2}\right) + v\frac{\partial^3 u}{\partial y^3} + \frac{\partial u}{\partial y}\frac{\partial^2 v}{\partial y^2}\right] - \frac{\sigma_{nf}B_0^2}{\rho_{nf}}(u - u_\infty), \tag{2}$$

Energy equation:

$$\frac{\partial T}{\partial t} + u\frac{\partial T}{\partial x} + v\frac{\partial T}{\partial y} = \frac{k_{nf}}{(\rho c)_{nf}}\frac{\partial^2 T}{\partial y^2} + \frac{\mu_{nf}}{(\rho c)_{nf}}\left(\frac{\partial u}{\partial y}\right)^2 + \frac{\alpha_1}{(\rho c)_{nf}}\left[\frac{\partial u}{\partial y}\frac{\partial^2 u}{\partial t \partial y} + u\frac{\partial u}{\partial y}\frac{\partial^2 u}{\partial x \partial y} + v\frac{\partial u}{\partial y}\frac{\partial^2 u}{\partial y^2}\right] + \tau_1\left[D_B\frac{\partial C}{\partial y}\frac{\partial T}{\partial y} + \frac{D_T}{T_\infty}\left(\frac{\partial T}{\partial y}\right)^2\right], \tag{3}$$

Nanoparticle Concentration Equation:

$$\frac{\partial C}{\partial t} + u\frac{\partial C}{\partial x} + v\frac{\partial C}{\partial y} = D_B\frac{\partial^2 C}{\partial y^2} + \frac{D_T}{T_\infty}\frac{\partial^2 T}{\partial y^2}, \tag{4}$$

here u and v are velocity components along x- and y-axis respectively. We further note that $\tau_1 = \frac{(\rho c)_p}{(\rho c)_{nf}}$ where $(\rho c)_{nf}$ and $(\rho c)_p$ are the heat capacities of nanofluid and nanoparticles respectively. The boundary conditions are defined following [49, 50] as:

$$\text{at } y = 0,\ v = 0,\ u(x, y, t) = u_w + u_{slip},\ T = T_w + N\frac{\partial T}{\partial y},\quad D_B\frac{\partial C}{\partial y} + \frac{D_T}{T_\infty}\frac{\partial T}{\partial y} = 0,$$

$$\text{as } y \to \infty,\ u \to u_\infty,\ T = T_\infty,\ C = C_\infty, \tag{5}$$

where velocity slip u_{slip} is defined by [51]:

$$u_{slip} = \frac{2}{3}\left(\frac{3 - \alpha_m l^3}{\alpha_m} - \frac{3}{2}\frac{1 - l^2}{Kn}\right)\lambda\frac{\partial u}{\partial y} - \frac{1}{4}\left(l^4 + \frac{2}{K_n^2}(1 - l^2)\right)\lambda^2\frac{\partial^2 u}{\partial y^2} = A\frac{\partial u}{\partial y} + B\frac{\partial^2 u}{\partial y^2}, \tag{6}$$

here $\alpha_m$represents momentum accommodation coefficient, $l = \min\left(\frac{1}{K_n}, 1\right)$, K_n is the Knudsen number and λ is mean free path. The values of α_m and l fall between 0 and 1.

To facilitate HAM solutions, it is pertinent to render the governing eqns. (2)–(4) and boundary conditions (5) into non-dimensional form. We invoke therefore the following similarity transformations [52]:

$$\eta = \sqrt{\frac{a}{\upsilon_{nf}\xi}}y,\ \psi = \sqrt{a\upsilon_{nf}\xi}xf(\eta, \xi),\ u = axf'(\eta, \xi),\ v = -\sqrt{a\upsilon_{nf}\xi}f(\eta, \xi),$$

$$\theta(\eta, \xi) = \frac{T - T_\infty}{T_w - T_\infty},\ \phi(\eta, \xi) = \frac{C - C_\infty}{C_\infty},\ \xi = 1 - e^{-\tau},\ \tau = at, \tag{7}$$

where η is similarity variable (transformed transverse co-ordinate), ψ is stream function defined by the Cauchy-Riemann equations, $u = \frac{\partial \psi}{\partial y}$ and $v = -\frac{\partial \psi}{\partial x}$, which satisfies the continuity eq. (1). Prime denotes the differentiation with respect to η. Applying transformations (7) to the governing eqns. (2)–(4) and boundary conditions (5), it may be shown that the following system of coupled, nonlinear dimensionless partial differential equations emerges:

$$[\xi - \alpha(1 - \xi)]f''' + \xi^2(ff'' - f'^2) - \xi^2(1 - \xi)\frac{\partial f'}{\partial \xi} + \frac{\eta}{2}\xi(1 - \xi)f'' + \alpha\left[\xi^2(1 - \xi)\frac{\partial f'''}{\partial \xi} + 2\xi f'f''' - \frac{\eta}{2}(1 - \xi)f^{iv}\right] - \alpha\xi(ff^{iv} + f''^2) + M^2\xi^2(1 - f') + \xi^2 = 0, \tag{8}$$

$$\frac{1}{\Pr}\left(\theta'' + Nb\theta'\phi' + Nt\theta'^2\right) + \xi f\theta' - \xi(1-\xi)\frac{\partial\theta}{\partial\xi} + \frac{\eta}{2}(1-\xi)\theta' + \alpha Ec\left[f'f''^2 - ff''f'''\right] + \alpha Ec(1-\xi)\left(f''\frac{\partial f''}{\partial\xi} - \frac{\eta}{2}\theta'\right) + Ecf''^2 = 0, \tag{9}$$

$$\phi'' + \frac{Nt}{Nb}\theta'' + Sc\left[\xi f\phi' - (1-\xi)\left(\xi\frac{\partial\phi}{\partial\xi} - \frac{\eta}{2}\phi'\right)\right] = 0. \tag{10}$$

The associated transformed boundary conditions are:

at $\eta = 0, f(0) = 0, f'(0) = \beta + \lambda_1 f''(0) + \lambda_2 f'''(0), \theta(0) = 1 + \delta\theta'(0),$

$$\text{as } Nb\,\phi'(0) + Nt\,\theta'(0) = 0,$$

$$\eta \to \infty, f'(\eta) = 1, \theta(\eta) = 0, \phi(\eta) = 0. \tag{11}$$

Here the following definitions apply: $\alpha = \frac{a\alpha_1}{\rho_{nf}\upsilon_{nf}}$, $M = \sqrt{\frac{\sigma_{nf}B_0^2}{a\rho_{nf}}}$, $\Pr = \frac{\upsilon_{nf}}{\alpha'}$, $Nb = \frac{\tau_1 D_B C_\infty}{\alpha'}$, $Nt = \frac{\tau_1 D_T(T_w - T_\infty)}{T_\infty\alpha'}$, $\alpha' = \frac{k_{nf}}{(\rho c)_{nf}}$, $Ec = \frac{u_w^2}{c_{nf}(T_w - T_\infty)}$, $Sc = \frac{\upsilon_{nf}}{D_B}$, $\lambda_1 = A\sqrt{\frac{a}{\upsilon_{nf}\xi}}$,

$$\lambda_2 = B\left(\frac{a}{\upsilon_{nf}\xi}\right), \delta = N\sqrt{\frac{a}{\upsilon_{nf}\xi}}, \beta = \frac{b}{a}. \tag{12}$$

Where α is second grade viscoelastic parameter, M is magnetic body force parameter, Pr is Prandtl number, Nb is Brownian motion parameter, Nt is thermophoretic parameter, α' is thermal diffusivity, Ec is Eckert number, Sc is Schmidt number, λ_1 and λ_2 are the first and second order slip velocity parameters, δ is thermal slip (jump) parameter and β is the stagnation parameter (values lie between 0 and 1).

2.1 Quantities of physical interest:

2.1.1 Skin friction coefficient:

The skin friction coefficient which provides an estimate of the surface shear stress, is defined as

$$C_{nf} = \frac{\tau_w}{\rho_{nf}(ax)^2}. \tag{13}$$

Here τ_w represents wall skin friction which may be defined as:

$$\tau_w = \mu_{nf}\left.\frac{\partial u}{\partial y}\right|_{y=0} + \alpha_1\left[u\frac{\partial^2 u}{\partial x\partial y} + v\frac{\partial^2 u}{\partial y^2} + 2\frac{\partial u}{\partial x}\frac{\partial u}{\partial y} + \frac{\partial^2 u}{\partial t\partial y}\right]_{y=0}. \tag{14}$$

After applying the similarity transformations on τ_w we have:

$$Cfr = \sqrt{\mathrm{Re}\xi}C_{nf} = f''(0,\xi) + \alpha\left[3f'(0,\xi)f''(0,\xi) + (1-\xi)\left(\frac{\partial f''(0,\xi)}{\partial\xi} - \frac{\eta}{2\xi}f''' - \frac{f''}{2\xi}\right)\right], \tag{15}$$

where Re is the Reynolds number.

2.1.2 Local Nusselt number:

The local Nusselt number Nu which evaluates the rate of heat transfer at the wall is given by the following expression:

$$Nu = \frac{xq_w}{k_{nf}(T_w - T_\infty)}. \tag{16}$$

Here q_w is wall heat flux defined as:

$$q_w = -k_{nf}\left.\frac{\partial T}{\partial y}\right|_{y=0} - h_p\rho_p\left(D_B\frac{\partial C}{\partial y} + \frac{D_T}{T}\frac{\partial T}{\partial y}\right)_{y=0}. \tag{17}$$

After applying similarity transformation and using the expressions of Nb and Nt, we obtain:

$$Nur = \sqrt{\frac{\xi}{\mathrm{Re}}}Nu = -\left[\theta'(0,\xi) + \left(Nb\phi'(0,\xi) + Nt\theta'(0,\xi)\right)\right] = -\theta'(0,\xi). \tag{18}$$

The simplification follows since $Nb\phi'(0,\xi) + Nt\theta'(0,\xi) = 0$.

3 Entropy Generation Analysis

Entropy generation analysis is the analysis of physical parameters on entropy generation number. We can control the wastage of useful energy with the help of this analysis. The local volumetric rate of entropy generation number for viscoelastic nanofluid in the presence of magnetic field is defined as [36, 53]:

$$S_G = \underbrace{\frac{k_{nf}}{T_\infty^2}\left(\frac{\partial T}{\partial y}\right)^2}_{I^{st}} + \underbrace{\frac{1}{T_\infty}\left[\mu_{nf}\left(\frac{\partial u}{\partial y}\right)^2 + \alpha_1\left(\frac{\partial u}{\partial y}\cdot\frac{\partial^2 u}{\partial y\partial t} + u\frac{\partial u}{\partial y}\frac{\partial^2 u}{\partial x\partial y} + v\frac{\partial u}{\partial y}\frac{\partial^2 u}{\partial y^2}\right)\right]}_{II^{nd}} + \underbrace{\frac{RD_B}{C_\infty}\left(\frac{\partial C}{\partial y}\right)^2 + \frac{RD_B}{T_\infty}\left(\frac{\partial T}{\partial y}\right)\left(\frac{\partial C}{\partial y}\right)}_{III^{rd}} + \underbrace{\frac{\sigma_{nf}B_0^2}{T_\infty}(u_\infty - u)^2}_{IV^{th}} = N_1 + N_2 + N_3 + N_4, \tag{19}$$

eq. (19) indicates the contribution of *four sources* of entropy generation. The first source of entropy generation,N_1, is the transfer of *heat across a finite temperature difference* and is embodied in the first term in eq. (19). The second term (N_2) is the source of entropy generation due to viscous dissipation. The third term (N_3) represents the source of entropy generation due to diffusion. Finally the fourth term (N_4) is entropy generation due to the effect of magnetic field. The dimensionless entropy generation number is defined as:

$$N_S = \frac{S_G}{S_c}, \tag{20}$$

here S_c is the characteristic entropy generation rate which for boundary condition (5), is defined as:

$$S_c = \frac{k_{nf}(\Delta T)^2}{x^2 T_\infty^2}. \tag{21}$$

Applying similarity transformations (7) on eq. (13) yields:

$$N_S = \frac{\mathrm{Re}}{\xi}\left[\theta'^2 + \frac{\mathrm{Pr}.Ec}{\Omega}\left\{f''^2 + \xi M^2(1-f')^2 + \alpha\left((1-\xi)\left(f''\frac{\partial f''}{\partial \xi} - \frac{\eta}{2\xi}f''f''' - \frac{f''^2}{2\xi}\right) + f'f''^2 - ff''f'''\right)\right\}\right] + \frac{\mathrm{Re}}{\xi}\frac{\chi}{\Omega}\left(\frac{1}{\Omega}\phi'^2 + \theta'\phi'\right), \tag{22}$$

where *Re* is Reynolds number, Ω is dimensionless temperature difference and χ is diffusive constant, which are defined, respectively, as:

$$\mathrm{Re} = \frac{ax^2}{\upsilon_{nf}}, \Omega = \frac{T_w - T_\infty}{T_\infty}, \chi = \frac{RD_B C_\infty}{k_{nf}}. \tag{23}$$

Bejan number [31] provides a way to determine whether the entropy generation due to heat transfer is dominant over total entropy generation or not. The Bejan number is utilized in this regard and is defined as:

$$\textit{Bejan number } Be = \frac{\text{Entropy generation due to heat transfer}}{\text{Total entropy generation}} = \frac{N_1}{N_S}. \tag{24}$$

The range of Bejan number lies between 0 and 1. When *Be* is close to 1, then entropy generation due to heat transfer dominates.

4 Homotopy Analysis Method (HAM) Solutions

We solve eqns. (8)–(11) analytically with the help of the homotopy analysis method (HAM). In this method, a set of *base functions* is selected which provides the base of a power series solution. On the basis of boundary conditions (11), we select the following set of base functions [43]:

$$\{\eta^k \xi^m \exp(-c\eta) \,|\, k \geq 0, c \geq 0, m \geq 0\}. \tag{25}$$

According to (25), we choose the following initial guesses, linear operators and auxiliary functions:

$$f_0(\eta,\xi) = \frac{\beta-1}{1+\lambda_1-\lambda_2}(1-\exp(-\eta)) + \eta,$$

$$\theta_0(\eta,\xi) = \frac{1}{1+\delta}\exp(-\eta), \phi_0(\eta,\xi) = -\frac{Nt}{Nb}\exp(-\eta),$$

$$L_f(f) = \frac{\partial^3 f}{\partial \eta^3} + \frac{\partial^2 f}{\partial \eta^2}, L_\theta(\theta) = \frac{\partial^2 \theta}{\partial \eta^2} + \frac{\partial \theta}{\partial \eta}, L_\phi(\phi) = \frac{\partial^2 \phi}{\partial \eta^2} + \frac{\partial \phi}{\partial \eta},$$

$$H_f(\eta,\xi) = H_\theta(\eta,\xi) = H_\phi(\eta,\xi) = 1, \tag{26}$$

where L_f, L_θ and L_ϕ satisfy the following conditions:

$$\begin{aligned} L_f(C_1 + C_2\eta + C_3 e^{-\eta}) &= 0, \\ L_\theta(C_4 + C_5 e^{-\eta}) &= 0, \\ L_\phi(C_6 + C_7 e^{-\eta}) &= 0, \end{aligned} \tag{27}$$

here C_1 toC_7 are constants. From eqns. (8)–(10), the *nonlinear operators* are defined as:

$$\begin{aligned} &N_f[\psi_f(\eta,\xi,q), \psi_\theta(\eta,\xi,q), \psi_\phi(\eta,\xi,q)] \\ &= [\xi - \alpha(1-\xi)]\psi'''_f(\eta,\xi,q) + \xi^2\psi_f(\eta,\xi,q)\psi''_f(\eta,\xi,q) \\ &- \xi^2(\psi'_f(\eta,\xi,q))^2 \\ &+ \xi(1-\xi)\left(\frac{\eta}{2}\psi''_f(\eta,\xi,q) - \xi\frac{\partial \psi'_f(\eta,\xi,q)}{\partial \xi}\right) \\ &+ \xi^2\left(M^2(1-\psi'_f(\eta,\xi,q)) + 1\right) \\ &+ \alpha\left((1-\xi)\left(\xi^2\frac{\partial \psi'''_f(\eta,\xi,q)}{\partial \xi} - \frac{\eta}{2}\psi^{iv}{}_f(\eta,\xi,q)\right)\right. \\ &\left.+2\xi\psi'_f(\eta,\xi,q)\psi'''_f(\eta,\xi,q) - \xi(\psi_f(\eta,\xi,q)\psi^{iv}{}_f(\eta,\xi,q))\right) \\ &- \alpha\xi\left[\psi''^2{}_f(\eta,\xi,q)\right], \end{aligned} \tag{28}$$

$$\begin{aligned} &N_\theta[\psi_f(\eta,\xi,q), \psi_\theta(\eta,\xi,q), \psi_\phi(\eta,\xi,q)] \\ &= \frac{1}{\mathrm{Pr}}\left(\psi''_\theta(\eta,\xi,q) + Nb\psi'_\theta(\eta,\xi,q)\psi'_\phi(\eta,\xi,q)\right. \\ &\left.+Nt\psi'^2{}_\theta(\eta,\xi,q)\right) + \xi\psi_f(\eta,\xi,q)\psi'_\theta(\eta,\xi,q) \\ &+ (1-\xi)\left(\frac{\eta}{2}\psi'_\theta(\eta,\xi,q) - \xi\frac{\partial \psi_\theta(\eta,\xi,q)}{\partial \xi}\right) \\ &+ \alpha Ec\left[(1-\xi)\psi''_f(\eta,\xi,q)\frac{\partial \psi_f(\eta,\xi,q)}{\partial \xi}\right] \\ &+ \alpha Ec\left(\psi'_f(\eta,\xi,q)\psi''^2{}_f(\eta,\xi,q)\right. \\ &\left.-\psi''_f(\eta,\xi,q)\psi'''_f(\eta,\xi,q)\left(\psi_f(\eta,\xi,q) + \frac{\eta(1-\xi)}{2}\right)\right) \\ &+ Ec\psi''^2{}_f, \end{aligned} \tag{29}$$

$$N_\phi[\psi_f(\eta,\xi,q),\psi_\theta(\eta,\xi,q),\psi_\phi(\eta,\xi,q)] = \psi''_\phi(\eta,\xi,q) + \left(\frac{Nt}{Nb}\right)\psi''_\theta(\eta,\xi,q) + Sc\left[\xi\psi_f(\eta,\xi,q)\psi'_\phi(\eta,\xi,q)\right] - Sc\,(1-\xi)\left(\xi\frac{\partial\psi_\phi(\eta,\xi,q)}{\partial\xi} - \frac{\eta}{2}\psi'_\phi(\eta,\xi,q)\right). \quad (30)$$

The *zero-order deformation* equations emerge as:

$$(1-q)L_f[\psi_f(\eta,\xi,q) - f_0(\eta,\xi)] = qh_fH_f(\eta,\xi)N_f[\psi_f(\eta,\xi,q),\psi_\theta(\eta,\xi,q),\psi_\phi(\eta,\xi,q)], \quad (31)$$

$$(1-q)L_\theta[\psi_\theta(\eta,\xi,q) - \theta_0(\eta,\xi)] = qh_\theta H_\theta(\eta,\xi)N_\theta[\psi_\theta(\eta,\xi,q),\psi_\theta(\eta,\xi,q),\psi_\phi(\eta,\xi,q)], \quad (32)$$

$$(1-q)L_\phi[\psi_\phi(\eta,\xi,q) - \phi_0(\eta,\xi)] = qh_\phi H_\phi(\eta,\xi)N_\phi[\psi_\phi(\eta,\xi,q),\psi_\theta(\eta,\xi,q),\psi_\phi(\eta,\xi,q)], \quad (33)$$

with boundary conditions

$$\begin{aligned}
&\psi_f(0,\xi,q) = 0,\\
&\psi'_f(0,\xi,q) = \beta + \lambda_1\psi''_f(0,\xi,q) + \lambda_2\psi'''_f(0,\xi,q),\\
&\psi'_f(\infty,\xi,q) = 1,\\
&\psi_\theta(0,\xi,q) = 1 + \delta\psi'_\theta(0,\xi,q),\\
&\psi'_\theta(\infty,\xi,q) = 0,\\
&Nb\psi_\phi{}'(0,\xi,q) + Nt\psi_\theta{}'(0,\xi,q) = 0,\\
&\psi'_\phi(\infty,\xi,q) = 0,
\end{aligned} \quad (34)$$

where h_f, h_θ, h_ϕ are non-zero auxiliary parameters, H_f, H_θ, H_ϕ are non-zero auxiliary functions and q is an *embedding parameter* which lies between 0 and 1. It is clear from (31)-(33) that, when

$$q = 0,\quad \psi_f(\eta,\xi,0) = f_0(\eta,\xi),\quad \psi_\theta(\eta,\xi,0) = \theta_0(\eta,\xi),\quad \psi_\phi(\eta,\xi,0) = \phi_0(\eta,\xi), \quad (35)$$

and when

$$q = 1,\ \psi_f(\eta,\xi,1) = f(\eta,\xi),\ \psi_\theta(\eta,\xi,1) = \theta(\eta,\xi),\ \psi_\phi(\eta,\xi,1) = \phi(\eta,\xi). \quad (36)$$

Expanding $f(\eta,\xi,q)$, $\theta(\eta,q)$ and $\phi(\eta,q)$via Taylor's series expansions in powers of q then we obtain

$$f(\eta,\xi,q) = f_0(\eta,\xi) + \sum_{m=1}^{\infty} f_m(\eta,\xi)q^m, \quad (37)$$

$$\theta(\eta,\xi,q) = \theta_0(\eta,\xi) + \sum_{m=1}^{\infty} \theta_m(\eta,\xi)q^m, \quad (38)$$

$$\phi(\eta,\xi,q) = \phi_0(\eta,\xi) + \sum_{m=1}^{\infty} \phi_m(\eta,\xi)q^m, \quad (39)$$

where

$$f_m = \frac{1}{m!}\frac{\partial^m\psi_f(\eta,\xi,q)}{\partial q^m}\bigg|_{q=0},\ \theta_m = \frac{1}{m!}\frac{\partial^m\psi_\theta(\eta,\xi,q)}{\partial q^m}\bigg|_{q=0} \text{ and } \phi_m = \frac{1}{m!}\frac{\partial^m\psi_\phi(\eta,\xi,q)}{\partial q^m}\bigg|_{q=0}. \quad (40)$$

Differentiating eqns. (31)–(33) m times with respect to q and dividing these by $m!$ and then substituting $q = 0$, we obtain:

$$L_f(f_m(\eta,\xi) - \chi_{m-1}f_{m-1}(\eta,\xi)) = h_fH_fR^f_m(\eta,\xi), \quad (41)$$

$$L_\theta(\theta_m(\eta,\xi) - \chi_{m-1}\theta_{m-1}(\eta,\xi)) = h_\theta H_\theta R^\theta_m(\eta,\xi), \quad (42)$$

$$L_\phi(\phi_m(\eta,\xi) - \chi_{m-1}\phi_{m-1}(\eta,\xi)) = h_\phi H_\phi R^\phi_m(\eta,\xi), \quad (43)$$

$$\begin{aligned}
&f_m(0,\xi) = 0, f'_m(0,\xi) - \lambda_1 f''_m(0,\xi) - \lambda_2 f'''_m(0,\xi) = 0,\\
&f'_m(\infty,\xi) = 0,
\end{aligned} \quad (44)$$

$$\theta_m(0,\xi) - \delta\theta'_m(0,\xi) = 0,\ \theta(\infty,\xi) = 0, \quad (45)$$

$$Nb\phi'(0,\xi) + Nt\theta'(0,\xi) = 0,\ \phi_m(\infty,\xi) = 0. \quad (46)$$

Eqs. (44)–(46) are called the m^{th} *order deformation equations*. In these equations the term $R^f_m(\eta,\xi)$, $R^\theta_m(\eta,\xi)$ and $R^\phi_m(\eta,\xi)$ are defined as:

$$\begin{aligned}
R^f_m(\eta,\xi) = \frac{1}{m-1!}\frac{\partial^{m-1}N_f}{\partial q^{m-1}}\bigg|_{q=0} &= \left[\xi - \alpha(1-\xi)\right]f'''_{m-1}\\
&+ \xi(1-\xi)\left(\frac{\eta}{2}f''_{m-1} - \xi\frac{\partial f'_{m-1}}{\partial\xi}\right) + \xi^2\sum_{i=0}^{m-1} f_{m-1-i}f''_i\\
&- \xi^2\sum_{i=0}^{m-1} f'_{m-1-i}f'_i + \alpha(1-\xi)\left(\xi^2\frac{\partial f'''_{m-1}}{\partial\xi} - \frac{\eta}{2}f^{iv}_{m-1}\right)\\
&- M^2\xi^2 f'_{m-1} - \alpha\xi\left[\sum_{i=0}^{m-1}\left(f_{m-1-i}f^{iv}_i + f''_{m-1-i}f''_i - 2f'_{m-1-i}f'''_i\right)\right]\\
&+ (M^2+1)\xi^2(1-\chi_m),
\end{aligned} \quad (47)$$

$$R_m^{\theta}(\eta,\xi) = \frac{1}{m-1!}\frac{\partial^{m-1}N_\theta}{\partial q^{m-1}}\bigg|_{q=0}$$
$$= \frac{1}{\Pr}\left(\theta_{m-1}^{''} + Nb\sum_{i=0}^{m-1}\theta_i^{'}\phi_{m-1-i}^{'} + Nt\sum_{i=0}^{m-1}\theta_i^{'}\theta_{m-1-i}^{'}\right)$$
$$+ (1-\xi)\left(\frac{\eta}{2}\theta_{m-1}^{'} - \xi\frac{\partial\theta_{m-1}}{\partial\xi}\right)$$
$$+ Ec\sum_{i=0}^{m-1}f_i^{''}f_{m-1-i}^{''} + \alpha Ec(1-\xi)\sum_{i=0}^{m-1}f_i^{''}\frac{\partial f''_{m-1-i}}{\partial\xi}$$
$$+\alpha Ec\left[\sum_{i=0}^{m-1}\sum_{j=0}^{i}\left(f_{m-1-i}^{'}f_{i-j}^{''}f_j^{''} - f_{m-1-i}f_{i-j}^{''}f_j^{'''}\right)\right]$$
$$- \frac{\eta(1-\xi)}{2}\sum_{i=0}^{m-1}f_i^{''}f_{m-1-i}^{'''} + \xi\sum_{i=0}^{m-1}f_i\theta_{m-1-i}^{'}, \tag{48}$$

$$R_m^{\phi}(\eta,\xi) = \frac{1}{m-1!}\frac{\partial^{m-1}N_\phi}{\partial q^{m-1}}\bigg|_{q=0} = \phi_{m-1}^{''} + \left(\frac{Nt}{Nb}\right)\theta_{m-1}^{''}$$
$$+ Sc\left[\xi\sum_{i=0}^{m-1}f_i\phi_{m-1-i}^{'} - (1-\xi)\left(\xi\frac{\partial\phi_{m-1}}{\partial\xi} - \frac{\eta}{2}\phi_{m-1}^{'}\right)\right], \tag{49}$$

and

$$\chi_m = \begin{array}{l} 0, m \le 1 \\ 1, m > 1 \end{array}\Bigg|. \tag{50}$$

We choose the values of auxiliary parameters h_f, h_θ, h_ϕ such that the appropriate series (37-39) are convergent at $q = 1$. Thus, using (35) and (36), we obtain the following power series solutions:

$$f(\eta,\xi,q) = f_0(\eta,\xi) + \sum_{m=1}^{\infty}f_m(\eta,\xi), \tag{51}$$

$$\theta(\eta,\xi,q) = \theta_0(\eta,\xi) + \sum_{m=1}^{\infty}\theta_m(\eta,\xi), \tag{52}$$

$$\phi(\eta,,\xi,q) = \phi_0(\eta,\xi) + \sum_{m=1}^{\infty}\phi_m(\eta,\xi). \tag{53}$$

We have used the symbolic software Maple 18 and obtain the m^{th} terms in the following form:

$$f_m(\eta,\xi) = F_m(\eta,\xi) + C_1 + C_2\eta + C_3e^{-\eta}, \tag{54}$$

$$\theta_m(\eta,\xi) = \Theta_m(\eta,\xi) + C_4 + C_5e^{-\eta}, \tag{55}$$

$$\phi_m(\eta,\xi) = \Phi_m(\eta,\xi) + C_6 + C_7e^{-\eta}, \tag{56}$$

here $F_m(\eta,\xi)$, $\Theta_m(\eta,\xi)$ and $\Phi_m(\eta,\xi)$ are the *particular* solutions. We calculate the values of constants C_1 to C_7 with the help of the boundary conditions (44)–(46).

Table 1: The values of $f'(0,\xi)$, $\theta(0,\xi)$ and $\phi'(0,\xi)$ for different order of approximations for the values of parameters $Nt = Nb = 0.5$, $Sc = 10$, $Ec = 0.5$, M = 0.5, $Pr = 5$, $\alpha = 0.2, \delta = 0.3, \lambda_1 = \lambda_2 = 0.1$, $\beta = 0.2, \xi = 0.8$, $h_f = -0.04$, $h_\theta = -0.009$, $h_S = -0.009$.

Order	$f'(0,\xi)$	$\theta(0,\xi)$	$\phi'(0,\xi)$
5	0.8630	0.7682	0.7723
10	0.8838	0.7677	0.7743
15	0.8901	0.7673	0.7755
20	0.8909	0.7672	0.7757
25	0.8909	0.7672	0.7557

4.1 Convergence of HAM Solutions

The convergence of HAM series solutions depends on the appropriate choice of initial guesses, linear operators, auxiliary functions and auxiliary parameters. We have already selected the initial guesses, linear operators and auxiliary functions. Liao [43] suggested that one can plot the *h-curves* to establish the appropriate value of auxiliary parameter h. For the present study, we have plotted the *h-curves* with $f''(0,\xi)$, $\theta'(0,\xi)$ and $\phi'(0,\xi)$for different orders of approximations, which are displayed in Figs. 2(a) – 2(c). To check the behavior of ξon the admissible range of the value of h_f , we have also plotted the *h-curve* with $f''(0,\xi)$ for different values of ξ which are displayed in Fig. 2(d). These figures illustrate that the adequate ranges for h_f, h_θ and h_ϕ are [–0.09, –0.028], [–0.022, 0] and [0.022, 0] respectively. The order of convergence of series of solution is represented in Table 1 for the values of auxiliary parameters $h_f = -0.04$, $h_\theta = h_\phi = -0.009$. This table shows that series of solutions are convergent up to the 20^{th} order of approximations.

5 Results and Discussion

Extensive computations have been performed with the homotopy analysis method (HAM). The influence of governing parameters such as magnetic parameter (M), second grade viscoelastic parameter (α), first and second order slip velocity parameter (λ_1 and λ_2), thermal slip parameter (δ) and stagnation parameter (β) (values lie between 0 to 1) on skin friction coefficient, rate of heat transfer, entropy generation number and Bejan number is visualized graphically in Figs. 3–8. To validate the HAM solutions, Table 2 provides a comparison of present HAM results with previous published results of Wang [54] in the limiting case of *non-magnetic, steady, Newtonian, no-slip flow*, and generally very good correlation is achieved between both results. HAM results for rate of heat transfer

$\{-\theta'(0,\xi)\}$up to the 15^{th} order of approximation is presented in Table 3 for different values of M, Pr, α and $\lambda_2$with the following default values for other parameters: $Nt = 0.5, Nb = 0.5, Ec = 0.5, Sc = 10, \beta = 0.2, \xi = 0.8$ and $\lambda_1 = 0.1, \delta = 0.3$. It is evident from Table 3 that $\{-\theta'(0,\xi)\}$ increases with an increasing the values of Prandtl number Pr but decreases with an increment in second grade viscoelastic parameter α, second order slip velocity parameter λ_2 and magnetic parameter M.

Table 2: Comparison between the present analytical results and published results of $f''(0,\xi)$ for $M = 0$, $\xi = 1$ (steady state), $\alpha = \lambda_1 = \lambda_2 = 0$.

β	Present values	Wang [54]
0	1.23279	1.232588
0.1	1.14679	1.14656
0.2	1.05160	1.05113
0.5	0.71361	0.71330
1	0	0

Fig. 3 displays the effects of second grade (viscoelastic) parameter, α, on Nusselt number and skin friction coefficient. Fig. 3(a) shows that skin friction coefficient decreases with an increment in the value of α for $\tau < 1$ but it shows an opposite behavior with α for $\tau > 1$. The influence of viscoelasticity parameter is therefore also dependent on the magnitude of time (τ). Viscoelasticity parameter, $\alpha = \frac{a\alpha_1}{\rho_{nf}\upsilon_{nf}}$, arises in many terms in the dimensionless momentum eq. (8) and also the viscous heating terms in the energy conservation eq. (9). It embodies the relative effects of fluid elasticity to viscosity in the nanofluid. As this parameter increases the contribution of elastic effects is increased which serves to decelerate the boundary layer flow and increase momentum boundary layer thickness, at lower times. The contrary response is computed at higher values of time. Elastico-viscous materials such as the second grade nanofluid exhibit normal stresses which modifies their response with time progression and indeed this is the case. Viscoelastic materials also generally possess a relaxation time. With lower viscoelastic parameter values, the viscous effects dominate rather than the elastic effects. The case of *$\alpha = 0$ corresponds to purely viscous flow (vanishing elastic effect)*.

Fig. 3(b) shows that Nusselt number consistently decreases with an increment in viscoelasticity parameter α. Greater elastic effect therefore decreases the rate of heat transfer to the wall at all time instants and a corresponding increase in the temperatures within the nanofluid boundary layer. This manifests in an increase in thermal boundary layer thickness.

Table 3: HAM values of Nusselt number $\{-\theta'(0,\xi)\}$for different values of magnetic parameter M, second grade viscoelastic parameter α and second order slip parameter λ_2, with all other parameters fixed and with order of approximations of fifteen.

		(α, λ_2)		
M	Pr	(0.1, 0.1)	(0.1, 0.2)	(0.2,0.2)
0.1	5	0.7768	0.7701	0.7692
	7	0.7812	0.7744	0.7736
	10	0.7845	0.7834	0.7769
0.3	5	0.7766	0.7755	0.7689
	7	0.7810	0.7741	0.7733
	10	0.7843	0.7774	0.7766

Figs. 4(a)–4(d) illustrate the effects of the parameters M, β, λ_1 and λ_2 against dimensionless time τ on skin friction coefficient. Increasing magnetic parameter (M) as observed in Fig. 4a, clearly enhances skin friction. Even though the transverse magnetic field generates a Lorentzian body force, owing to the fact that the magnetic field is *moving with the free stream velocity*, the overall contribution is assistive to the velocity field. This accelerates the boundary layer flow and enhances skin friction values at all times. This effect has been observed by several researchers in magnetohydrodynamics including Zueco *et al.* [55]. We can further understand the effect of magnetic field on velocity from the term $\frac{\sigma_{nf}B_0^2}{\rho_{nf}}(u - u_\infty)$ in the eq. (2). It contains two terms, the first term $\frac{\sigma_{nf}B_0^2}{\rho_{nf}}u$ represents the Lorentz force (retarding force) and the second term $\frac{\sigma_{nf}B_0^2}{\rho_{nf}}u_\infty$ represents the imposed pressure force from the outer region of boundary layer. In our analysis, we consider the outer flow velocity as higher than boundary layer velocity ($u_\infty > u$), the term $\frac{\sigma_{nf}B_0^2}{\rho_{nf}}(u - u_\infty)$ will become negative, thus the magnetic field increases the velocity in the boundary region and effectively the skin-friction at the surface (which is a function of velocity gradient) increases with magnetic field. Fig. 4b shows that skin friction coefficient decreases with an increasing in the value of stagnation parameter (β) i.e. momentum boundary layer thickness is increased owing to flow deceleration. Fig. 4c indicates that skin friction coefficient is also decreased with greater first order velocity slip parameter (λ_1). However in Fig. 4d it is apparent that flow acceleration accompanies an increase in second order velocity slip parameter (λ_2) and therefore that momentum boundary layer thickness in the nanofluid is reduced.

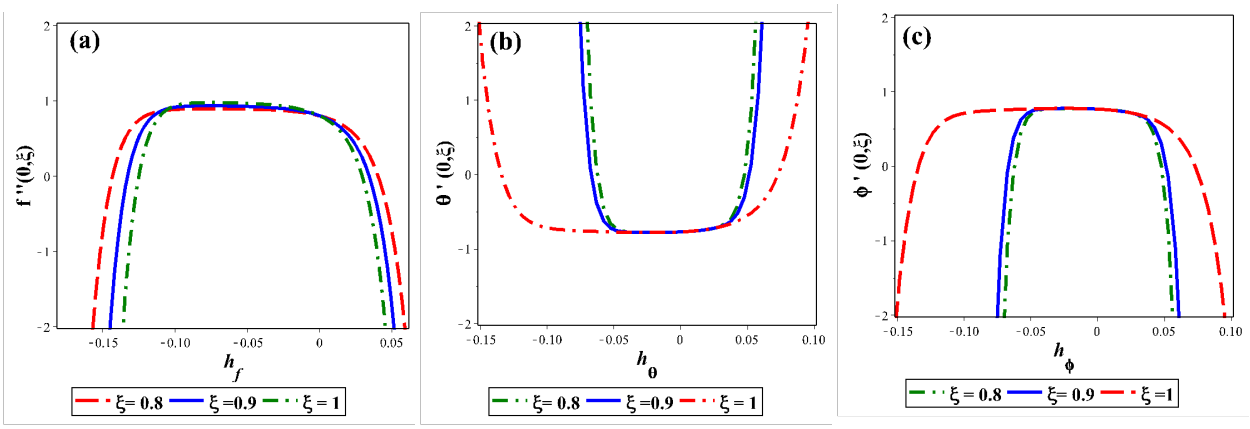

Fig. 2: Validation of *h-values* of $f''(0)$, $\theta'(0)$and$\phi'(0)$ for different values of ξ (order = 10).

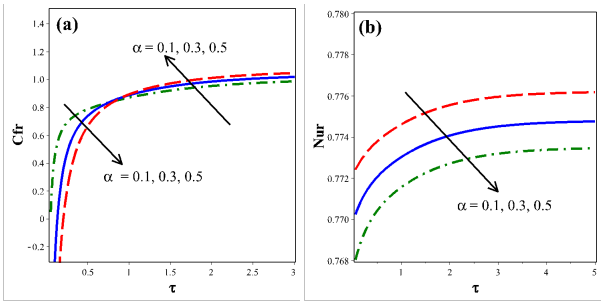

Fig. 3: Effect of second grade parameter on skin friction coefficient and Nusselt number.

Figs. 5(a)–5(c) depict the effects of the dissipation parameter, Eckert number (Ec), stagnation parameter (β) and thermal slip parameter (δ) on rate of heat transfer $\{-\theta'(0,\xi)\}$ with dimensionless time (τ). These figures illustrate that the increment in the value of *Ec* and δ lead to a depression in heat transfer $\{-\theta'(0,\xi)\}$ whereas the velocity parameter β favors the heat transfer $\{-\theta'(0,\xi)\}$. Increasing Eckert number implies a greater conversion in mechanical energy to thermal energy (i.e. dissipation of heat). This energizes the boundary layer and elevates temperatures, also increasing thermal boundary layer thickness. Heat is therefore drawn away from the wall into the boundary layer which manifests in a reduction in Nusselt number as shown in fig. 5a. Greater stagnation parameter implies larger velocity ratio i.e. greater stretching sheet velocity to ambient nanofluid velocity (β = b/a = u_w/u_∞, as discussed earlier). This enhances momentum diffusion and accelerates the boundary layer flow which boosts the skin friction values (Fig. 5b) i.e. the nanofluid shears faster along the wall. Greater thermal slip will enhance temperatures within the boundary layer (increase thermal boundary layer thickness) which will decrease the rate of heat transfer to the wall i.e. reduce Nusselt number as seen in Fig. 5c.

Figs. 6(a)–6(d) depict the influence of Reynolds number *Re*, magnetic parameter *M*, second grade viscoelastic parameter α and thermal slip parameter δ on entropy generation number N_S against η. These figures demonstrate that N_S decreases near the surface of sheet whereas with greater η the distributions plateau i.e. they remain invariant with transverse coordinate after a critical value. Fig. 6(a) indicates that entropy generation number N_S increases with an increment in Reynolds number *Re*. With greater Reynolds number, the inertial (momentum) force in the regime exceeds the viscous force, which serves to increases the disorderness in movement of fluid and encourages an entropy increase. The steep decrement in the entropy has been noticed as move away from the wall within the boundary layer regime, then after minimum stable value is achieved far from the boundaries.

Fig. 6(b) shows that with greater magnetic parameter *M* there is a notable enhancement in N_S. With greater magnetic parameter, the effect of the Lorentz magnetohydrodynamic body forces increase and this elevates the rate of heat transfer (temperature gradient) at the wall. Since N_S is a function of gradient of temperature effectively stronger magnetic field effect elevates N_S values. The effect of second grade viscoelastic parameter α on N_S is presented in Fig. 6(c) from which it is apparent that N_S is an increasing function of α i.e. greater elastic effects encourage entropy generation. Fig. 6(d) however shows that N_S is a decreasing function of thermal slip parameter δsince this parame-

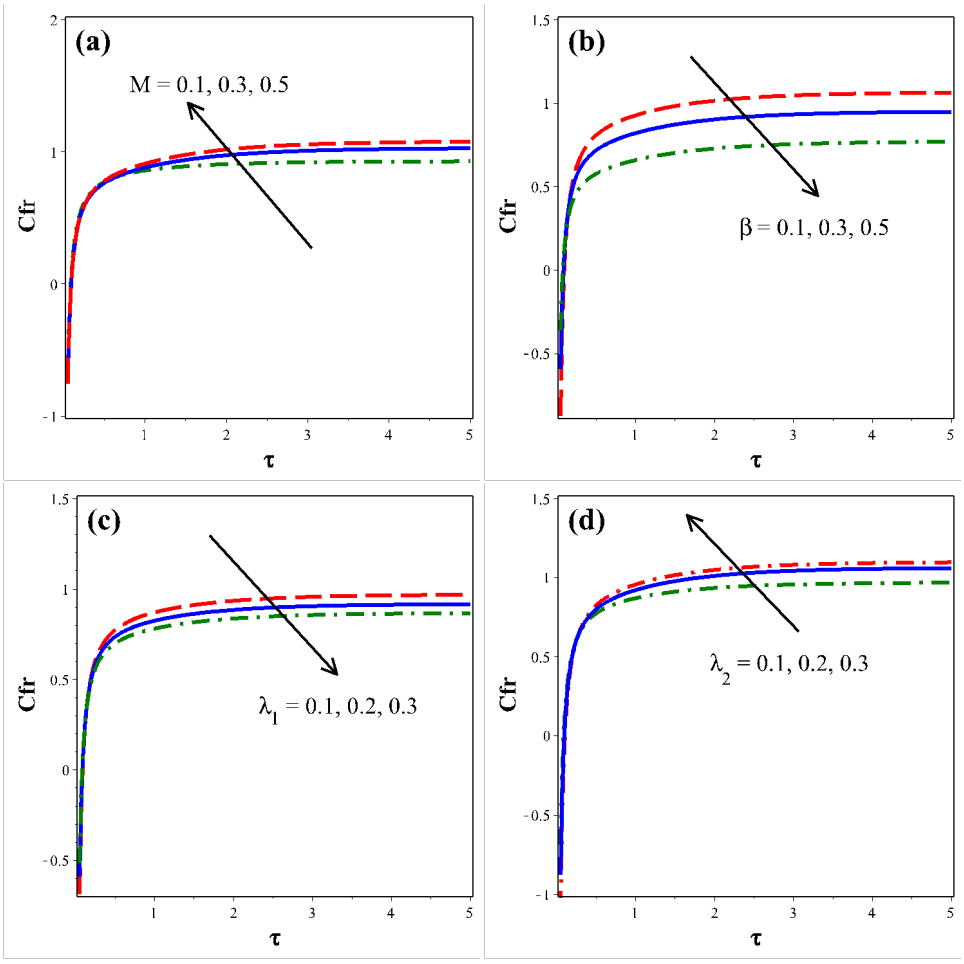

Fig. 4: Influence of magnetic parameter, stagnation parameter, first and second order slip velocities parameters on skin friction coefficient.

ter heats the boundary layer and reduces temperature gradient at the wall, to which N_S is proportional.

Figs. 7(a)–7(c) depict the influence of M, α and δ on Bejan number, Be. Bejan number Be is a dimensionless number signifying the ratio of entropy generation due to heat transfer to the total entropy generation. Typically Bejan numbers assume values between 0 and 1. If Be is very close to 1, this physically implies that entropy generation due to heat transfer dominates. Inspection of the figures reveals that Be generally decreases with an increasing values of M and δ and α. In the vicinity of sheet surface Bejan number increases for a short distance into the boundary layer, with an increasing the value of α. However very quickly the dominant influence as with magnetic parameter M, and thermal slip parameter δ, is a strong reduction in Bejan number. Generally in all the plots the free stream i.e. far from the stretching sheet the Bejan number plummets to zero, whereas the maximum Bejan number arises closer to the wall.

Figs. 8(a)–8(c) represent the combined effects of governing parameters (Re, χ), (M, α) and (Nt, Nb)on entropy generation parameter (Ns). The combined effects of Reynolds number Re and diffusive constant parameter χ are shown in Fig. 8(a), and it is apparent that entropy is the increasing function of these parameters. The combined effects of magnetic parameter M and viscoelastic parameter α on entropy generation are shown in Fig. 8(b) and again entropy is found to be enhanced by both parameters, in consistency with the results computed in Fig. 6(b) and 6(c). Fig. 8(c) shows the behavior of Nt and Nb on entropy which indicates that Ns is increased with an increment in the value of thermophoresis parameter (Nt) with the converse trend computed with increasing Brownian motion parameter Nb. Increasing Brownian motion parameter physically implies smaller nanoparticles which enhances temperatures but reduces wall temperature gradient (heat transfer rate at the wall). This serves to decrease entropy generation parameter (Ns). On the other hand the temperature gradient increases with thermphoresis pa-

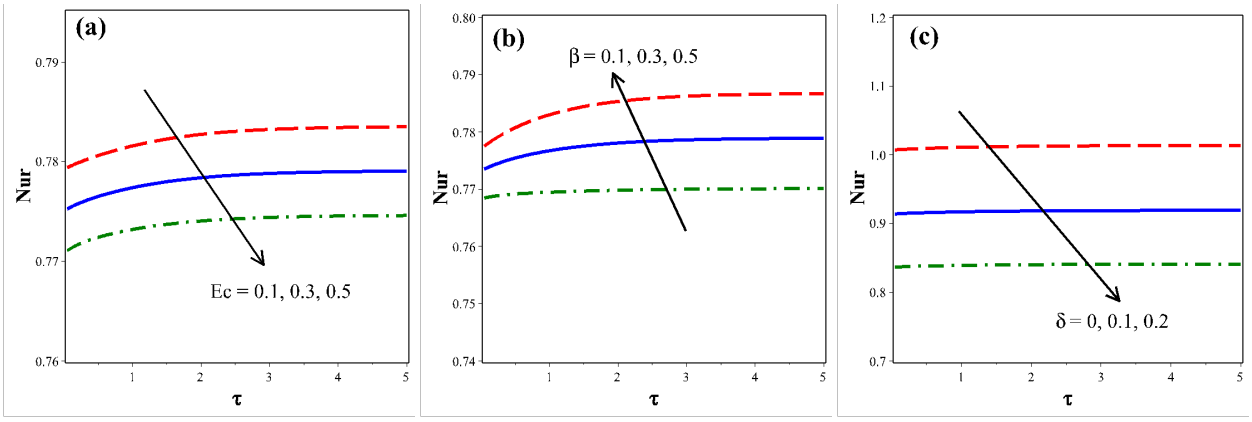

Fig. 5: Influence of Eckert number, stagnation parameter and thermal slip parameter on Nusselt number.

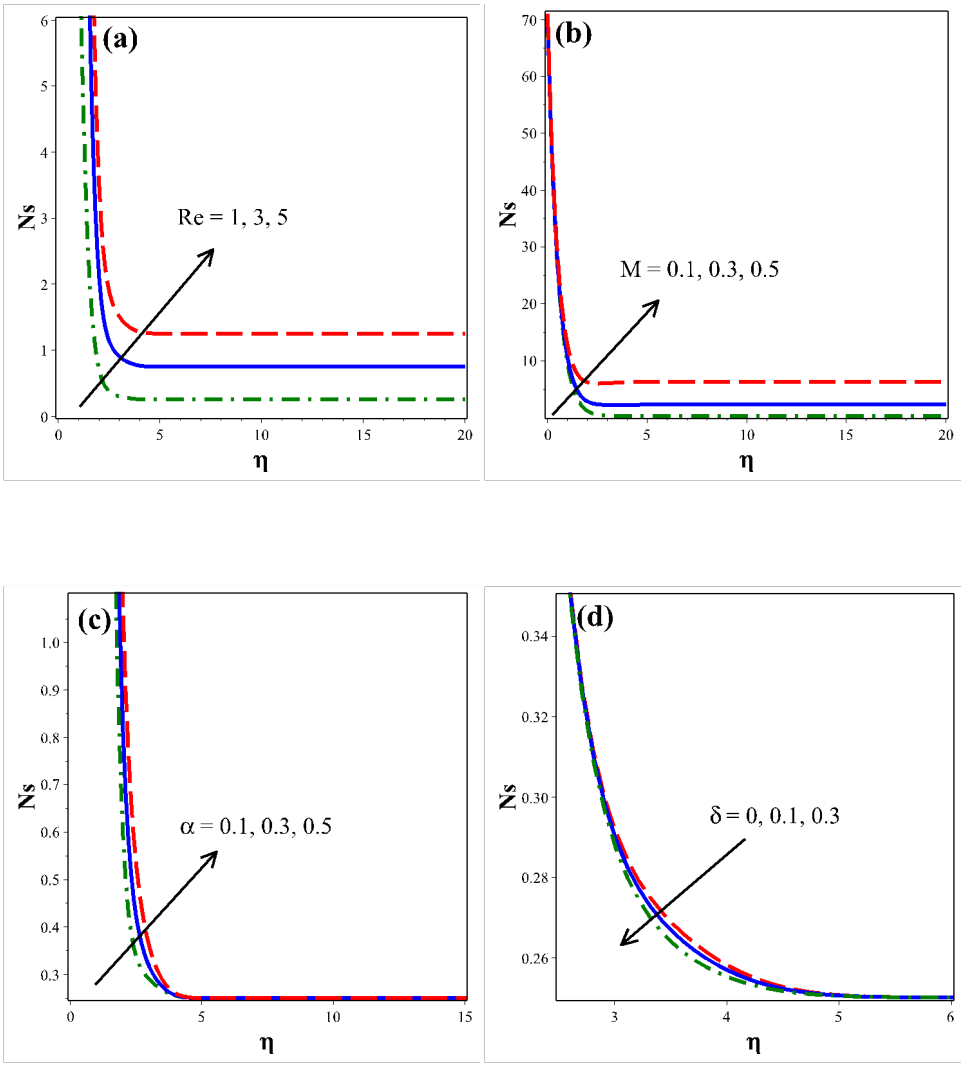

Fig. 6: Influence of Reynolds number, magnetic parameter, second grade parameter and thermal slip parameter on entropy generation number.

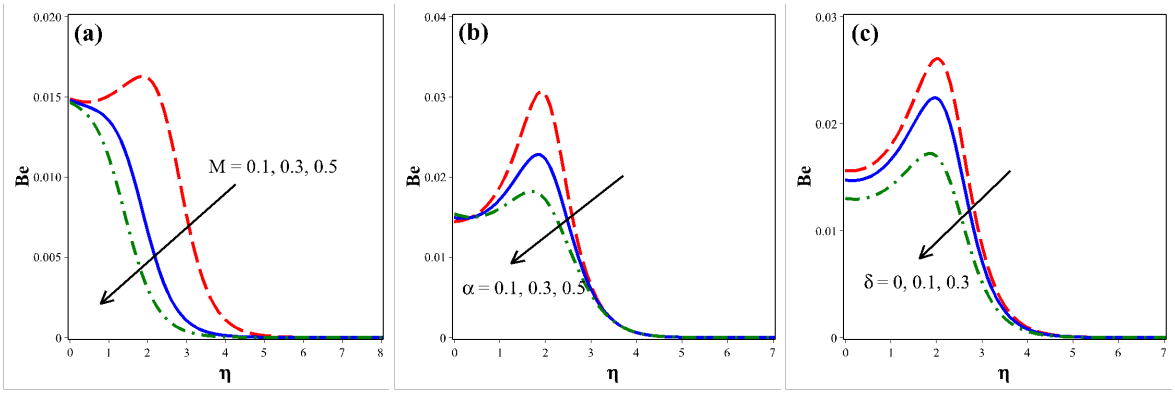

Fig. 7: Influence of magnetic parameter, second grade parameter and thermal slip on Bejan number *Be*.

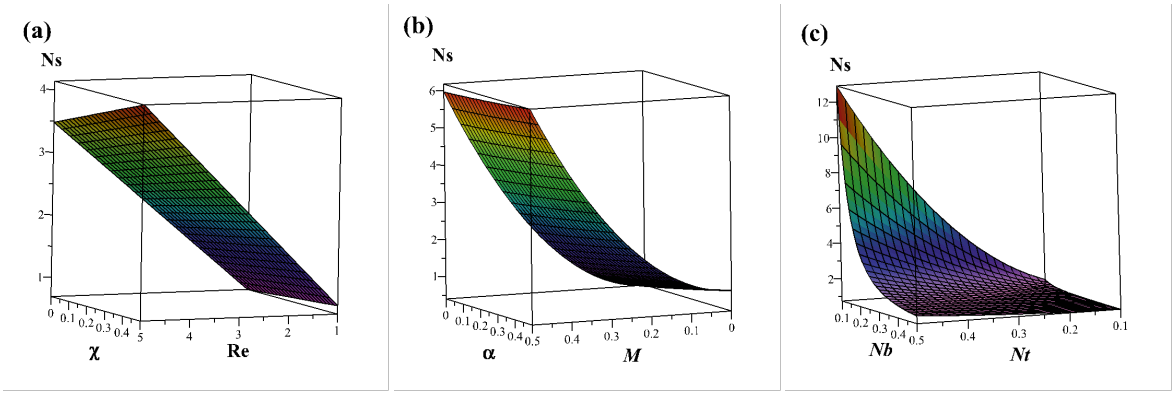

Fig. 8: Combined effects of physical parameters on entropy generation parameter.

rameter *Nt* and this favors entropy generation leading to an elevation in *Ns* values.

6 Concluding Remarks

The present study has developed a mathematical model for time-dependent MHD boundary layer stagnation point heat and mass transfer in second grade nanofluid flow over a horizontal stretching sheet. At the boundary, second order slip velocity and thermal slip effects have been considered with no-flux nanoparticles condition. Homotopy analysis method (HAM) solutions have been derived for the transformed, dimensionless two-point nonlinear boundary value problem. The effects of governing parameters such as magnetic parameter M, Eckert number Ec, second grade viscoelastic parameter α, first and second order slip velocity parameter λ_1 and λ_2, thermal slip parameter δ and velocity ratio (stagnation) parameter β on skin friction coefficient, Nusselt number, entropy generation number and Bejan number have been visualized and interpreted in detail. The present computations have shown that:

- Skin friction coefficient increases with M and λ_2, but decreases with an increase in the value of β and λ_1.
- Nusselt number decreases with an increase in the value of thermal slip and Eckert number whereas it increases with an increment in β.
- Entropy generation number is enhanced with an increase in Reynolds number Re, magnetic parameter M, and second grade viscoelastic parameter α whereas it is decreased with an increment in δ.
- Bejan number which represents the ratio entropy due to heat transfer to total entropy, reduces with M and δ. It increases with an increase in viscoelastic parameter α.
- Entropy generation parameter is increased with Reynolds number *Re*, diffusive constant parameter, χ, magnetic parameter M, viscoelastic parameter α and Brownian motion parameter, *Nb*, whereas it is increased with thermophoresis parameter, Nt.

The present work has confirmed the adaptability of HAM for solving nonlinear non-Newtonian magnetic nanofluid transport problems with entropy generation and alternative rheological models (e.g. micropolar) will be examined in the future [56].

Nomenclature

k	Thermal conductivity (W/m-K)	t	Time (s)
a, b	constant (s^{-1})	u_w	Velocity of sheet (m/s)
B_0	Magnetic field strength (Teslas)	T_∞	Ambient temperature (K)
C	Nanoparticle volume fraction (–)	Nb	Brownian motion parameter (–)
C_∞	Ambient volume fraction (–)	Nt	Thermophoresis parameter (–)
D_B	Brownian diffusion coefficient (m^2/s)	Pr	Prandtl number (–)
D_T	Thermophoretic diffusion coefficient (m^2/s)	K_n	Knudsen number (–)
Ec	Eckert number (–)	R	Gas constant(J $mol^{-1}K^{-1}$)
f	Dimensionless stream function (–)	T	Nanofluid temperature (K)
		T_w	Nanofluid temperature at surface (K)
A	A constant in velocity slip model(m)	L	A constant (–)
B	A constant in velocity slip model (m^2)	q_w	Wall heat flux(W)
N	Thermal slip factor (–)	u, v	Velocity components along x-axis and y-axis (m/s)
M	Dimensionless Magnetic field parameter (–)	Sc	Schmidt number (–)
Re	Reynolds number (–)	x, y	Cartesian coordinates (m)
	Greek symbol		
η	Similarity variables (–)	$(\rho c)_f$	Heat capacity of nanofluid (J/K-m^3)
μ	Dynamic viscosity (Ns/m^2)	$(\rho c)_p$	Effective heat capacity of nanoparticle material (J/K-m^3)
ϕ	Dimensionless nanoparticle concentration (–)	χ	Diffusive constant parameter (–)
θ	Dimensionless temperature (–)	τ	Dimensionless time (–)
ν	Kinematic viscosity (m^2/s)	α_1	Viscoelastic parameter (kg/m)
α	Second grade viscoelastic parameter (–)	Ω	Dimensionless temperature difference(–)
λ	Molecular mean free path (m)	ψ	Stream function (m^2/s)
β	Stagnation parameter	ρ	Density (Kg/m^3)
λ_1,λ_2	First and second order velocity slip parameters (–)	σ	Electric conductivity of nanofluid (S/m)
δ	Thermal slip parameter (–)	α_m	Momentum accommodation coefficient (–)
	Subscript		
∞	Ambient condition	nf	Nanofluid
w	Condition on surface	p	Nanoparticle

References

[1] S.J. Liao, On the analytic solution of magnetohydrodynamic flows of non-Newtonian fluids over a stretching sheet, Journal of Fluid Mechanics. 2003, 488, 189–212.

[2] S. Nadeem, R.U. Haq, Z.H. Khan, Numerical solution of non-Newtonian nanofluid flow over a stretching sheet, Applied Nanoscience. 2014, 4, 625–631.

[3] S.U.S. Choi, J.A. Eastman, Enhancing thermal conductivity of fluids with nanoparticles, Argonne National Lab., IL (United States), 1995.

[4] J. Buongiorno, Convective Transport in Nanofluids, ASME Journal of Heat Transfer. 2006, 128, 240–250.

[5] A. Zeeshan, N. Shehzad, R. Ellahi, Analysis of activation energy in Couette-Poiseuille flow of nanofluid in the presence of chemical reaction and convective boundary conditions, Results in Physics. 2018, 8, 502–512.

[6] K. Milani Shirvan, R. Ellahi, M. Mamourian, M. Moghiman, Effects of wavy surface characteristics on natural convection heat transfer in a cosine corrugated square cavity filled with nanofluid, International Journal of Heat and Mass Transfer. 2017, 107, 1110–1118.

[7] K. Milani Shirvan, M. Mamourian, S. Mirzakhanlari, R. Ellahi, Numerical investigation of heat exchanger effectiveness in a double pipe heat exchanger filled with nanofluid: A sensitivity analysis by response surface methodology, Powder Technology. 2017, 313, 99–111.

[8] R. Ellahi, M.H. Tariq, M. Hassan, K. Vafai, On boundary layer nano-ferroliquid flow under the influence of low oscillating stretchable rotating disk, Journal of Molecular Liquids. 2016.

[9] M. Hassan, A. Zeeshan, A. Majeed, R. Ellahi, Particle shape effects on ferrofuids flow and heat transfer under influence of low oscillating magnetic field, Journal of Magnetism and Magnetic Materials. 2017, 443, 36–44.

[10] P. Rana, R. Dhanai, L. Kumar, MHD slip flow and heat transfer of Al2O3-water nanofluid over a horizontal shrinking cylinder using Buongiorno's model: Effect of nanolayer and nanoparticle diameter, Advanced Powder Technology. 2017, 28, 1727–1738.

[11] E. Erdogan, C.E. Imrak, Steady circulatory flow of a second grade fluid about a rotating porous cylinder, International Journal of Engineering Science. 2010, 48, 1225–1232.

[12] D. Zhang, S. Feng, Z. Lu, Y. Liu, Exact solutions for steady flows of second-grade fluids, Journal of Shanghai University (English Edition). 2009, 13, 340–344.

[13] P. Rana, R. Bhargava, Finite element simulation of transport phenomena of viscoelastic nanofluid over a stretching sheet with energy dissipation, Journal of Information and Operations Management. 2012, 3, 158–161.

[14] M. Khurana, P. Rana, S. Srivastava, Influence of the combined effect of magnetic field and rotation on the onset of a non-Newtonian viscoelastic nanofluid layer: Linear and nonlinear analyses, The European Physical Journal Plus. 2016, 131, 437.

[15] M. Anwari, Sukarsan, Performance characteristic of Faraday MHD accelerator: Effect of magnetic field to the thrust, in:

2008 IEEE Veh. Power Propuls. Conf. 2008, 1–6.
[16] V.S. Bajović, A reliable tool for the design of shape and size of Faraday segmented MHD generator channel, Energy Conversion and Management. 1996, 37, 1753–1764.
[17] R. Dhanai, P. Rana, L. Kumar, Critical values in slip flow and heat transfer analysis of non-Newtonian nanofluid utilizing heat source/sink and variable magnetic field: Multiple solutions, Journal of the Taiwan Institute of Chemical Engineers. 2016, 58, 155–164.
[18] P. Rana, M.J. Uddin, Y. Gupta, A.I.M. Ismail, Two-component modeling for non-Newtonian nanofluid slip flow and heat transfer over sheet: Lie group approach, Applied Mathematics and Mechanics. 2016, 37, 1325–1340.
[19] K. Hiemenz, Die Grenzschicht an einem in den gleichförmigen Flüssigkeitsstrom eingetauchten geraden Kreiszylinder., Polytechnisches Journal. 1911, 326, 391–393.
[20] T. Hayat, M.S. Anwar, M. Farooq, A. Alsaedi, MHD Stagnation Point Flow of Second Grade Fluid over a Stretching Cylinder with Heat and Mass Transfer, International Journal of Nonlinear Sciences and Numerical Simulation. 2014, 15, 365–376.
[21] C.A. Reddy, B. Shankar, Magneto Hydrodynamics Stagnation Point Flow of a Nano Fluid over an Exponentially Stretching Sheet with an Effect of Chemical Reaction, Heat Source and Suction/Injunction, World Journal of Mechanics. 2015, 05, 211–221.
[22] N. Bachok, A. Ishak, I. Pop, The boundary layers of an unsteady stagnation-point flow in a nanofluid, International Journal of Heat and Mass Transfer. 2012, 55, 6499–6505.
[23] M. Suali, N. Long, N.M. A, N.M. Ariffin, Unsteady Stagnation Point Flow and Heat Transfer over a Stretching/Shrinking Sheet with Suction or Injection, Journal of Applied Mathematics. 2012, 1–12.
[24] Z. Abbas, M. Sheikh, I. Pop, Stagnation-point flow of a hydromagnetic viscous fluid over stretching/shrinking sheet with generalized slip condition in the presence of homogeneous–heterogeneous reactions, Journal of the Taiwan Institute of Chemical Engineers. 2015, 55, 69–75.
[25] P. Rana, M.J. Uddin, Y. Gupta, A.I.M. Ismail, Slip effects on MHD Hiemenz stagnation point nanofluid flow and heat transfer along a nonlinearly shrinking sheet with induced magnetic field: multiple solutions, Journal of the Brazilian Society of Mechanical Sciences and Engineering. 2017, 39, 3363–3374.
[26] A. Yoshimura, R.K. Prud'homme, Wall Slip Corrections for Couette and Parallel Disk Viscometers, Journal of Rheology. 1988, 32, 53–67.
[27] Y. Zhu, S. Granick, No-Slip Boundary Condition Switches to Partial Slip When Fluid Contains Surfactant, Langmuir. 2002, 18, 10058–10063.
[28] L. Wu, A slip model for rarefied gas flows at arbitrary Knudsen number, Applied Physics Letters. 2008, 93, 253103.
[29] T. Fang, S. Yao, J. Zhang, A. Aziz, Viscous flow over a shrinking sheet with a second order slip flow model, Communications in Nonlinear Science and Numerical Simulation. 2010, 15, 1831–1842.
[30] G. Singh, A.J. Chamkha, Dual solutions for second-order slip flow and heat transfer on a vertical permeable shrinking sheet, Ain Shams Engineering Journal. 2013, 4, 911–917.
[31] A. Bejan, Method of entropy generation minimization, or modeling and optimization based on combined heat transfer and thermodynamics, Revue Générale de Thermique. 1996, 35, 637–646.
[32] D.S. Herbein, W.M. Rohsenow, Comparison of entropy generation and conventional method of optimizing a gas turbine regenerator, International Journal of Heat and Mass Transfer. 1988, 31, 241–244.
[33] J. Esfahani, M. Akbarzadeh, S. Rashidi, M. Rosen, R. Ellahi, Influences of wavy wall and nanoparticles on entropy generation over heat exchanger plat, International Journal of Heat and Mass Transfer. 2017, 109, 1162–1171.
[34] S. Rashidi, S. Akar, M. Bovand, R. Ellahi, Volume of fluid model to simulate the nanofluid flow and entropy generation in a single slope solar still, Renewable Energy. 2018, 115, 400–410.
[35] A. Bejan, A Study of Entropy Generation in Fundamental Convective Heat Transfer, Journal of Heat Transfer. 1979, 101, 718–725.
[36] S. Aïboud, S. Saouli, Second law analysis of viscoelastic fluid over a stretching sheet subject to a transverse magnetic field with heat and mass transfer, Entropy. 2010, 12, 1867–1884.
[37] M.H. Abolbashari, N. Freidoonimehr, F. Nazari, M.M. Rashidi, Analytical modeling of entropy generation for Casson nanofluid flow induced by a stretching surface, Advanced Powder Technology. 2015, 26, 542–552.
[38] A.S. Butt, S. Munawar, A. Mehmood, A. Ali, Effect of Viscoelasticity on Entropy Generation in a Porous Medium over a Stretching Plate, n.d.
[39] A. Noghrehabadi, M.R. Saffarian, R. Pourrajab, M. Ghalambaz, Entropy analysis for nanofluid flow over a stretching sheet in the presence of heat generation/absorption and partial slip, Journal of Mechanical Science and Technology. 2013, 27, 927–937.
[40] S. Das, S. Chakraborty, R.N. Jana, O.D. Makinde, Entropy analysis of unsteady magneto-nanofluid flow past accelerating stretching sheet with convective boundary condition, Applied Mathematics and Mechanics. 2015, 36, 1593–1610.
[41] S. Jafarmadar, N. Azizinia, N. Razmara, F. Mobadersani, Thermal analysis and entropy generation of pulsating heat pipes using nanofluids, Applied Thermal Engineering. 2016, 103, 356–364.
[42] S.J. Liao, On the Proposed Homotopy Analysis Techniques for Nonlinear Problems and Its Applications, Shanghai Jiao Tong University, 1992.
[43] S.J. Liao, Beyond Perturbation: Introduction to the Homotopy Analysis Method, Chapman & Hall/CRC Press, London/Boca Ratton, 2003.
[44] F. Mabood, W.A. Khan, A.I.M. Ismail, MHD flow over exponential radiating stretching sheet using homotopy analysis method, Journal of King Saud University - Engineering Sciences. 2017, 29, 68–74.
[45] F. Mabood, W.A. Khan, Homotopy analysis method for boundary layer flow and heat transfer over a permeable flat plate in a Darcian porous medium with radiation effects, Journal of the Taiwan Institute of Chemical Engineers. 2014, 45, 1217–1224.
[46] B. Raftari, F. Parvaneh, K. Vajravelu, Homotopy analysis of the magnetohydrodynamic flow and heat transfer of a second grade fluid in a porous channel, Energy. 2013, 59, 625–632.
[47] M. Hassani, M. Mohammad Tabar, H. Nemati, G. Domairry, F. Noori, An analytical solution for boundary layer flow of a nanofluid past a stretching sheet, International Journal of Thermal Sciences. 2011, 50, 2256–2263.

[48] Z. Abbas, T. Hayat, M. Sajid, S. Asghar, Unsteady flow of a second grade fluid film over an unsteady stretching sheet, Mathematical and Computer Modelling. 2008, 48, 518–526.
[49] J. Zhu, L. Zheng, L. Zheng, X. Zhang, Second-order slip MHD flow and heat transfer of nanofluids with thermal radiation and chemical reaction, Applied Mathematics and Mechanics. 2015, 36, 1131–1146.
[50] K.-L. Hsiao, Stagnation electrical MHD nanofluid mixed convection with slip boundary on a stretching sheet, Applied Thermal Engineering. 2016, 98, 850–861.
[51] R. Sharma, A. Ishak, Second order slip flow of cu-water nanofluid over a stretching sheet with heat transfer, WSEAS Transactions on Fluid Mechanics. 2014, 9, 26–33.
[52] M. Sajid, I. Ahmad, T. Hayat, M. Ayub, Unsteady flow and heat transfer of a second grade fluid over a stretching sheet, Communications in Nonlinear Science and Numerical Simulation. 2009, 14, 96–108.
[53] S. Das, S. Chakraborty, R.N. Jana, O.D. Makinde, Entropy analysis of unsteady magneto-nanofluid flow past accelerating stretching sheet with convective boundary condition, Applied Mathematics and Mechanics. 2015, 36, 1593–1610.
[54] C.Y. Wang, Stagnation flow towards a shrinking sheet, International Journal of Non-Linear Mechanics. 2008, 43, 377–382.
[55] J. Zueco, O.A. Bég, H.S. Takhar, V.R. Prasad, Thermophoretic hydromagnetic dissipative heat and mass transfer with lateral mass flux, heat source, Ohmic heating and thermal conductivity effects: Network simulation numerical study, Applied Thermal Engineering. 2009, 29, 2808–2815.
[56] S. Jangili, N. Gajjela, O. Anwar Bég, Mathematical modeling of entropy generation in magnetized micropolar flow between co-rotating cylinders with internal heat generation, Alexandria Engineering Journal. 2016, 55, 1969–1982.